© 2019. Published by The Company of Biologists Ltd | Journal of Experimental Biology (2019) 222, jeb192518. doi:10.1242/jeb.192518

RESEARCH ARTICLE

A novel mechanism of mixing by pulsing corals

Julia E. Samson[1,*], Laura A. Miller[1,2,*,‡], Dylan Ray[2,§], Roi Holzman[3,4,§], Uri Shavit[4,5,§] and Shilpa Khatri[6,*]

ABSTRACT

The dynamic pulsation of xeniid corals is one of the most fascinating phenomena observed in coral reefs. We quantify for the first time the flow near the tentacles of these soft corals, the active pulsations of which are thought to enhance their symbionts' photosynthetic rates by up to an order of magnitude. These polyps are approximately 1 cm in diameter and pulse at frequencies between approximately 0.5 and 1 Hz. As a result, the frequency-based Reynolds number calculated using the tentacle length and pulse frequency is on the order of 10 and rapidly decays as with distance from the polyp. This introduces the question of how these corals minimize the reversibility of the flow and bring in new volumes of fluid during each pulse. We estimate the Péclet number of the bulk flow generated by the coral as being on the order of 100–1000 whereas the flow between the bristles of the tentacles is on the order of 10. This illustrates the importance of advective transport in removing oxygen waste. Flow measurements using particle image velocimetry reveal that the individual polyps generate a jet of water with positive vertical velocities that do not go below 0.1 cm s^{-1} and with average volumetric flow rates of approximately 0.71 cm^3 s^{-1}. Our results show that there is nearly continual flow in the radial direction towards the polyp with only approximately 3.3% back flow. 3D numerical simulations uncover a region of slow mixing between the tentacles during expansion. We estimate that the average flow that moves through the bristles of the tentacles is approximately 0.03 cm s^{-1}. The combination of nearly continual flow towards the polyp, slow mixing between the bristles, and the subsequent ejection of this fluid volume into an upward jet ensures the polyp continually samples new water with sufficient time for exchange to occur.

KEY WORDS: Soft corals, Xeniidae, Biomechanics, Computational fluid dynamics, Lagrangian particle tracking

INTRODUCTION

Flow is important to all aspects of life in the benthos, including feeding, respiration and reproduction (Nowell and Jumars, 1984). Benthic organisms, however, must cope with benthic boundary layers on the order of 1 m or more (Shashar et al., 1996; Reidenbach et al., 2006) that result from the no-slip condition (or zero flow) at the ocean's floor. Within the boundary layer, there tends to be significantly less mass transport, and vertically stratified regions may develop in which mixing is low and nutrient depletion and/or waste accumulation occur (Vogel, 1994). This can become a problem for small organisms contained within the boundary layer as they may have difficulty gathering nutrients from their environment or getting rid of waste products. Two main strategies exist to avoid this problem: increase size or adapt behavior. Organisms that increase in size may extend (partly) out of the boundary layer, ensuring that at least part of their surface is exposed to regions of high mixing. Behavioral adaptations to life in the boundary layer include the generation of jets (Santhanakrishnan et al., 2012), the use of cilia or flagella to create local flows (Petersen, 2007; Nielsen et al., 2017), or any other behavior resulting in increased fluid mixing and thus local reduction in boundary layer thickness.

At the polyp to colony scales, corals depend on ambient flows for exchange, but the xeniid corals (i.e. *Xenia* and *Heteroxenia*) generate their own flows. The flower-like polyps perpetually pulsate nonsynchronously. The function of this pulse was long thought to be for the purpose of feeding and prey capture (Lewis, 1982). However, several studies report the recurring absence of food particles in the guts of xeniid polyps (Gohar, 1940a,b; Fabricius and Alderslade, 2001) and suggest other methods of nutrient uptake such as endocytosis of food particles and absorption of dissolved nutrients (Schlichter, 1982). There have also been direct observations of xeniid corals failing to feed or even rejecting any solid particle that made its way inside the mouth (Gohar, 1940a,b; Lewis, 1982). Additional details of the morphology and behavior of these corals can be found in Gohar (1940a,b) and Gohar and Roushdy (1959).

More recently, Kremien et al. (2013) demonstrated that the collective pulsing of many soft coral polyps significantly alters the boundary layer in which they live. They also showed that pulsation increased gross photosynthesis rates by approximately 5-fold compared with non-pulsating colonies. They suggested that instead of a supply of nutrients and dissolved inorganic carbon (DIC), the role of the tentacle pulsations is to remove the excess oxygen resulting from the photosynthetic activity of the coral symbionts. Without pulsing behavior, this excess oxygen would accumulate in the coral tissue and this accumulation would decrease the affinity of RuBisCO (an enzyme involved in carbon fixation) to CO_2, reducing or even halting photosynthesis. At night, the same movement is thought to reduce hypoxic stress and avoid re-filtration of nutrient-depleted water (Kremien et al., 2013). These results suggest that by actively mixing their environment, these soft corals can thrive in sheltered and slow-flow habitats. The mechanism by which mixing is enhanced, however, is unclear.

Although most corals would benefit from improved oxygen removal during daytime and increased nutrient and DIC fluxes during the night, active flow generation within the diffusive boundary layer (< 1 mm scale) among corals is usually limited to the microscale. Many coral species possess epidermal cilia, the beating of which can break the diffusive boundary layer near the coral tissue and increase the mass transfer of oxygen from the tissue (Shapiro et al., 2014). At the centimeter to meter scales

[1]Biology Department, University of North Carolina at Chapel Hill, Chapel Hill, NC 27599, USA. [2]Department of Mathematics, University of North Carolina at Chapel Hill, Chapel Hill, NC 27599, USA. [3]School of Zoology, Tel Aviv University, Tel Aviv 6997801, Israel. [4]Inter-University Institute for Marine Sciences, Eilat 8810302, Israel. [5]Faculty of Civil and Environmental Engineering, Technion-Israel Institute of Technology, Haifa 3200003, Israel. [6]Department of Applied Mathematics, School of Natural Sciences, University of California, Merced, Merced, CA 95343, USA.
*These authors contributed equally to this work
§These authors contributed equally to this work

‡Author for correspondence (Lam9@unc.edu)

L.A.M., 0000-0003-3707-9798; R.H., 0000-0002-2334-2551

Received 13 October 2018; Accepted 12 July 2019

Journal of Experimental Biology (2019) 222, jeb192518. doi:10.1242/jeb.192518

(corresponding to the momentum and benthic boundary layers), mass transport through the colony is governed by larger-scale processes such as the formation of wakes and eddies as the ambient flow interacts with the coral reef (Falter et al., 2016; Bilger and Atkinson, 1992). Canopy and community mass transfer rates are positively correlated to the hydrodynamic bottom stresses in experimental and field corals and algae (Falter et al., 2016), indicating that the adaptations of corals to increasing mass flux are mainly structural and morphological.

Although the flow profiles above entire colonies of xeniid corals have been described by Kremien et al. (2013), the kinematics of the pulse has not been quantified, the flow fields generated by individual polyps have not been measured, and as a result, the importance of advection on removing oxygen waste has not been well characterized. How these and other benthic organisms experience their physical environment depends on their size, shape and local physical parameters including fluid velocity, density, viscosity and temperature. One straightforward way to quantify and compare organism-generated flows is through the use of dimensionless numbers (Vogel, 1998). For benthic organisms, two relevant dimensionless numbers include the Reynolds number and the Péclet number.

The Reynolds number, *Re*, is the ratio between inertial and viscous forces in a fluid, and is defined as:

$$Re = \frac{\rho L U}{\mu}, \quad (1)$$

where ρ is the fluid density in kg m^{-3}, *L* is a characteristic length (often taken as the greatest length of an object in the direction of the fluid flow; Vogel, 1994, 2013) in m, *U* is the free-stream flow velocity in m s^{-1}, and μ is the fluid's dynamic viscosity in Pa s^{-1} or kg (m s^{-1})$^{-1}$. When *Re*=1, inertial and viscous forces are balanced, when *Re*>1, inertial forces dominate, and when *Re*<1, viscous forces dominate. As can be seen in Eqn 1, the *Re* depends on the size of the organism and its relative velocity to the surrounding fluid. The relevant characteristic length and velocity used to calculate *Re* may vary to describe different aspects of the flow. To describe the bulk flow around a coral colony, the diameter of the colony may be chosen as the characteristic length and the background flow velocity as the characteristic velocity. To describe the *Re* of a pulsing organism, a frequency-based Reynolds number, Re_f, may be chosen, which is defined as:

$$Re_f = \frac{\rho L^2 f}{\mu}, \quad (2)$$

where *L* is the length of the appendage being moved (e.g. a tentacle) in m and *f* is the frequency in s^{-1} with which it is moved.

The Péclet number, *Pe*, describes the ratio of advective transport to diffusive transport for a given substance in flow and is defined as:

$$Pe = \frac{LU}{D}, \quad (3)$$

where *L* is the characteristic length in cm, *U* is a characteristic velocity in cm s^{-1} and *D* is the diffusion coefficient of the given substance in cm^2 s^{-1} (Vogel, 2013). An organism operating at high *Pe* can rely on advection (by swimming, pulsing, paddling, etc.) to influence mass transfer of nutrients and gases because the advective transport rate is significantly larger than the diffusive transport rate for the mass under consideration. Conversely, a low *Pe* indicates that diffusion prevails and that spending energy is less effective in gaining access to more nutrients or getting rid of waste products (Vogel, 2013).

In addition to generating sufficient flow to achieve advective transport, it is critical that at the polyp scale within the momentum boundary layer (*Pe*>>1), new volumes of fluid be brought to the organism during each cycle. At low *Re*, reciprocal motions generate reversible flows, and an organism would simply resample the same volume of fluid. For this reason, active reciprocal motions such as those used by the xeniid corals are relatively common among macroscopic marine animals operating at higher *Re*, with examples ranging from the active contractions of jellyfish bells for swimming (Dabiri et al., 2006; Costello and Colin, 1995; Hoover et al., 2017) and feeding (Santhanakrishnan et al., 2012; Peng and Dabiri, 2009) to fast contraction of the mantle for jet propulsion in squid, octopuses and other cephalopods (Gosline and DeMont, 1985; Bartol et al., 2008), and fast contraction of the shell in scallops (Manuel and Dadswell, 1993). Most examples that have been studied in detail occur at scales at which inertial forces in the fluid dominate over viscous forces, more specifically when the Re_f is on the order of 100 or more and the flow is non-reversible. There are interesting cases of organisms that use reciprocal motions at $1<Re_f<100$, particularly during ontogeny (Childress and Dudley, 2004; Katija et al., 2015; Ngo and McHenry, 2014; Murphy et al., 2016). An interesting feature of pulsing soft corals is that exchange jets are produced at scales where viscous forces in the fluid becomes non-negligible ($Re_f \approx 10$), and the use of reciprocal motions for propulsion and the generation of feeding currents becomes less efficient (Childress and Dudley, 2004; Alben and Shelley, 2005; Hamlet et al., 2011; Herschlag and Miller, 2011). It is therefore unclear how xeniid corals use reciprocal motion to generate efficient mixing and bring in new volumes of fluid. Accordingly, the movements of individual pulsing soft corals may generate interesting fluid dynamics that push the limits of mixing jets into the viscous regime, inspiring the design of efficient small-scale mixers.

The goal of this study was to determine how pulsing corals bring in new volumes of fluid during each pulse to enhance exchange despite being relatively small in size (<1 cm) and operating at relatively low *Re*. Furthermore, this work determined the relative importance of advection at various scales, ranging from the bulk flow generated by the polyp to the flows between the individual bristles on the tentacles. This paper includes the first quantitative analysis of the pulsing behavior of soft corals and the flows they generate. We used high-speed particle imaging velocimetry (PIV) to characterize the flows generated by xeniid coral polyps. This technique provided detailed measurements of the flows above the polyp. However, PIV measurements of the flow between the pulsating tentacles are difficult to obtain owing to limited optical access. We therefore conducted intensive three-dimensional simulations using the immersed boundary method (IBM) to model the flows between the tentacles. The regions of overlapping data for the two techniques were used to validate the three-dimensional simulations.

MATERIALS AND METHODS

Corals

Xeniid coral polyps were collected from the Red Sea at the Interuniversity Institute for Marine Sciences in Eilat, Israel. The corals were maintained in a water table at 24°C with water taken directly from the Red Sea.

Kinematics acquisition and reconstruction

Each polyp was filmed with a single camera at 125 or 60 frames s^{-1} in a quiescent fluid using a Photron SA3 120K camera. Tentacles

Journal of Experimental Biology (2019) 222, jeb192518. doi:10.1242/jeb.192518

with motions that were normal to the camera were tracked for kinematic analysis. Any motion in the third dimension was neglected. In each frame of the video, six different points (approximately equispaced) were marked along a tentacle using a MATLAB tool developed for kinematic measurement, DLTdv5 (Hedrick, 2008), as well as one other point at the opposite end of the base (Fig. S1; blue points). Based on the location of the two points on the base, the coral was then rotated to be in a vertical position. A cubic polynomial was then fit to the six points in each frame (Fig. S1; cyan curve). The fitting procedure sometimes required a slight rotation to make the fit more functional. From this cubic polynomial, the arclength of each of the tracked points along the tentacle was measured. Therefore, in each frame, the x-position, the y-position and the arclength of each tracked point along the tentacle were determined. Using these data, we non-dimensionalized the positions along the tentacles using the length of the tentacle in each frame. Using non-dimensionalized values allowed us to average over various tentacles and polyps. Cubic polynomials were then fit to the non-dimensional x- and y-positions as functions of the non-dimensional arclength (Fig. S1; red curve).

The pulse was divided into three phrases: contraction (tentacles closing), expansion (tentacles opening) and relaxation (negligible movement). Using the x- and y-positions of the points tracked on each tentacle from each frame, the motion for each phase was approximated using polynomials with time-varying coefficients. The cubic polynomial coefficient fits are shown for one tentacle for five pulses in Fig. S2. Included in each phase was four frames from the previous phase and four frames from the next phase to include some continuity between phases. The time was non-dimensionalized using the duration of the phase. To mathematically describe an averaged motion, these best-fit polynomials were determined using the position over time of one tentacle on five different polyps from two different colonies for five pulses. The resulting polynomials were then averaged to produce the motion. The averaged kinematics were then used to prescribe the preferred motion of the tentacles in the numerical simulations. It was assumed that all tentacles move with the same motion.

Particle image velocimetry (PIV)

Data were collected from two different colonies. In both cases, the camera was focused on one polyp to resolve the flow through the central axis of that particular polyp. One of the colonies consisted of only one polyp, and the other of four polyps. PIV videos were taken along the vertical (stem) axis of the chosen polyp, at the center of the polyp (sagittal plane). The particles used were glass beads of 10 µm diameter (Potter Industries). We used the same Photron SA3 120 K camera at 125 frames s^{-1} with a 105 mm NIKKOR lens. The camera was operated using the Photron FASTCAM Viewer software. The laser used was a continuous Genesis MX 523−8000 with a custom-built optical system that included an uncoated bi-concave lens (diameter=25.4 mm, f=−25.0 mm), an uncoated plano-convex lens (diameter=25.4 mm, f=75.0 mm) and a mounted plano-convex round cylindrical lens (diameter=25.4 mm, f=50 mm). The average thickness of the laser sheet was approximately 0.7 mm. The wavelength of the laser was 532 nm, and it was operated at approximately 2 W.

No pre-processing of the images was performed. PIV calculations were performed using the freely accessible OpenPIV package in Python (Taylor et al., 2010) with interrogation and search window sizes of 32×32 pixels and an overlap of 16 pixels. The polyp and its reflections from the laser were automatically masked. Note that this prevented the quantification of flow fields close to the tentacles. This problem is difficult to avoid given the opacity and reflective nature of the polyps, and is a major motivation for performing numerical simulations. Post-processing of the velocity vector fields involved interpolation to fill in rejected vectors. The signal-to-noise function in OpenPIV was applied with a threshold of 1.7 such that if the signal-to-noise ratio was below this value, the vector was replaced with the local mean. Large extraneous vectors were removed by replacing the top 1% in magnitude vectors with an average of neighboring velocity vectors.

Immersed boundary method

The unsteady, viscous and three-dimensional Navier–Stokes equations describing the fluid motion with an immersed elastic boundary representing the coral were numerically solved using the immersed boundary method (IBM) (Peskin, 2002). The IBM is a powerful tool for simulating biological fluid–structure interactions as it allows one to solve the fully coupled problem: the boundary both applies a force to the fluid and is deformed by fluid forces. Since its introduction by Peskin over 40 years ago (Peskin, 1972), the IBM has been used and extended to successfully model a variety of problems in biological fluid dynamics at intermediate scales ($10^{-2}<Re<1000$) including insect flight (Miller and Peskin, 2009), lamprey swimming (Tytell et al., 2014), cardiac blood flow (Peskin and McQueen, 1996; Gao et al., 2017) and the formation of blood clots by platelet aggregation (Skorczewski et al., 2014).

Here, we outline the immersed boundary method in three dimensions. For a full review of the method, see Peskin (2002). The equations of fluid motion are given by the Navier–Stokes equations:

$$\rho(\mathbf{u}_t(\mathbf{x},t)+\mathbf{u}(\mathbf{x},t)\cdot\nabla\mathbf{u}(\mathbf{x},t)) = -\nabla p(\mathbf{x},t)+\mu\nabla^2\mathbf{u}(\mathbf{x},t)+\mathbf{F}(\mathbf{x},t), \quad (4)$$

$$\nabla\cdot\mathbf{u}(\mathbf{x},t) = 0, \quad (5)$$

where $\mathbf{u}(\mathbf{x},t)$ is the fluid velocity, $p(\mathbf{x},t)$ is the pressure, $\mathbf{F}(\mathbf{x},t)$ is the force per unit volume applied to the fluid by the immersed boundary, ρ is the density of the fluid, and μ is the dynamic viscosity of the fluid. The independent variables are the time t and the position $\mathbf{x}$.

The interaction equations between the fluid and the boundary are given by:

$$\mathbf{F}(\mathbf{x},t) = \int \mathbf{f}(r,t)\delta(\mathbf{x}-\mathbf{X}(r,t))\mathrm{d}r, \quad (6)$$

$$\mathbf{X}_t(r,t) = \mathbf{U}(\mathbf{X}(r,t)) = \int \mathbf{u}(\mathbf{x},t)\delta(\mathbf{x}-\mathbf{X}(r,t))\mathrm{d}\mathbf{x}, \quad (7)$$

where $\mathbf{f}(r,t)$ is the force per unit area applied by the boundary to the fluid as a function of Lagrangian position and time, $\delta(\mathbf{x})$ is a three-dimensional delta function, and $\mathbf{X}(r,t)$ gives the Cartesian coordinates at time t of the material point labeled by the Lagrangian parameter r. Eqn 6 applies force from the boundary to the fluid grid, and Eqn 7 evaluates the local fluid velocity at the boundary. The boundary is then moved at the local fluid velocity, and this enforces the no-slip boundary condition. Each of these equations involves the three-dimensional Dirac delta function, δ, which acts as the kernel of an integral transformation. These equations convert Lagrangian variables to Eulerian variables and vice versa. An overview that provides the physical intuition behind the immersed boundary method is provided in Battista et al. (2015).

We prescribe the position of the coral using boundary points tethered to target points. Note that this is the preferred position, such that the actual boundary is within dx of the target position. The equation describing the force applied to the fluid by the

Journal of Experimental Biology (2019) 222, jeb192518. doi:10.1242/jeb.192518

boundary in Lagrangian coordinates is given by:

$$\mathbf{f}(r,t) = k_{\text{targ}}(\mathbf{Y}(r,t) - \mathbf{X}(r,t)), \quad (8)$$

where $\mathbf{f}(r,t)$ is the force per unit area, k_{targ} is a stiffness coefficient, and $\mathbf{Y}(r,t)$ is the prescribed position of the target boundary. k_{targ} is selected to ensure that the position of each boundary point is within $L_T/50$ (where L_T is the length of the tentacle) of its preferred or target location. As described above in the kinematics, we have developed an appropriate model for the moving coral based on video footage. The prescribed position of the target boundary is determined from this motion of the coral.

One of the main advantages of the IBM is that it is a straightforward way to handle the interaction between a fluid and an immersed structure with complex moving geometry. A Cartesian grid that is uniform throughout the domain can be used to solve the equations of fluid motion with a standard fluid solver. The immersed boundary, in our case the body of the soft corals, is represented by a collection of Lagrangian markers that move independently from this grid. The effect of the motion of the immersed boundary is transferred to the fluid grid through a simple-to-implement local stencil near each marker point. The IBM does not require a non-uniform or moving mesh. An adaptive and parallelized version of the IBM, IBAMR (https://github.com/IBAMR/IBAMR; Griffith et al., 2009), was used for all numerical simulations presented in this paper. IBAMR is a C++ library that provides discretization and solver infrastructure for partial differential equations on block-structured locally refined Eulerian grids (Berger and Oliger, 1984; Berger and Colella, 1989) and on Lagrangian (structural) meshes. IBAMR also includes infrastructure for coupling Eulerian and Lagrangian representations.

The adaptive Eulerian grid on which the Navier–Stokes equations were solved was locally refined near the immersed boundaries and regions of vorticity with a threshold of $|\omega|>0.1$. This Cartesian grid was organized as a hierarchy of four nested grid levels, and the finest grid was assigned a spatial grid size of $dx=D/1024$, where D is the length of the domain. The ratio of the spatial grid size on each grid relative to the next coarsest grid was 1:4. The parameters used for the simulations are given in Table 1.

Computational model

We report in this section the absolute physical values used in the immersed boundary simulations. The polyp-specific values are taken as the average experimental values. Variations in the experimental measurements are reported in the Results and were not incorporated into numerical simulations. The computational domain was set to be a 6×6×6 cm cube with periodic boundary conditions in the x- and y-directions and no-slip boundary conditions in the z-direction. The coral was placed in the bottom center of the computational domain and consisted of eight tentacles and a base. We did not include a stem because simulations show that the flow in this region near the central axis and below the base is negligible (less than 1% of the average flow around the polyp). This was also confirmed from PIV. The base of the tentacles was positioned 0.5 cm above the bottom of the domain, approximately the length of the stem of the polyp. The distance from the center of the polyp to the tip of a tentacle when the coral was fully extended was approximately 0.45 cm. The distance from the bottom of the polyp to the tip of the tentacles when the coral was fully contracted was 0.37 cm. The length of the tentacle was determined by averaging the length measured in each frame for each polyp and then averaging over all five polyps.

Each tentacle was assumed to have the shape of an isosceles trapezoid, where the width of the tentacle at its base was set to the average width across all measured polyps or 0.108 cm. This average was found by measuring the width of the bottom of the tentacle in one frame from each video when a tentacle was parallel to the plane of focus and could be clearly observed. This distance was then used to construct the numerical tentacle as long as it was not larger than one-eighth of the circumference of the base (in which case one-eighth of the circumference was used). The width of the top of the tentacle was set to be 0.2 times the width of the bottom. This factor prevented the overlap of the tentacles during the full contraction. The average diameter of the base of the polyp was determined by first measuring the distance between the bottoms of two oppositely arranged tentacles in each video frame. An average across all frames was taken to estimate the diameter of each polyp's base. These diameters were then averaged over all five polyps to obtain the average base diameter as 0.11 cm.

Table 1. Numerical and physical parameters used in the immersed boundary simulations

Name	Variable	Units	Value
Domain size	D	cm	6
Spatial grid size	dx	cm	5.86×10^{-3}
Boundary grid size	ds	cm	2.93×10^{-3}
Total simulation time	T_{tot}	pulses	10
Time step size	dt	s	1.22×10^{-4}
Fluid density	ρ	kg m^{-3}	1.0×10^{-3}
Fluid dynamic viscosity	μ	kg ms^{-1}	1.0×10^{-3}
Target point stiffness	k_{target}	kg m^{-3} s^{-2}	9.0×10^{-9}
Tentacle length	L_T	cm	0.41
Pulsing period	T	s	1.9

Data analysis

For the comparisons of the numerical simulations to experimentally measured flow fields using PIV, 2D uniform velocity fields were interpolated on a plane through the central axis of the numerical coral using Visit 2.12.3 (Childs et al., 2012). Visit was also used to graph velocities and vorticity. Tecplot 360 (https://www.tecplot.com/) was used to calculate the instantaneous streamlines. To quantitatively compare the flow fields, average velocities in the horizontal (radial) direction towards the coral and in the vertical direction above the coral were calculated from the experimental and computational data. The vertical velocity in the upward jet was averaged along a line in the x–y plane at the height of the tentacle tips during full contraction as well as at positions that were approximately one-half and one full tentacle length above that height. The horizontal velocity towards the polyp was averaged at the tentacle tips during full expansion as well as at positions that were approximately one-half and one full tentacle length to the left of that position.

We computed the finite-time Lyapunov exponent (FTLE) to determine Lagrangian coherent structures (LCSs) (Haller, 2002; Shadden et al., 2006) using Visit 2.12.3 (Childs et al., 2012). LCSs can reveal particle transport patterns in the flow field that are of potential biological importance, for example in predator–prey interactions and locomotion (Peng and Dabiri, 2009). In particular, Lagrangian coherent structures inform us about regions of the flow that are attractive (small FTLE) or repellant (large FTLE) (Shadden et al., 2005). By revealing the regions of fluid that repel or are 'separated', one can understand which portions of the fluid are sampled by the organism and which portions pass by the animal without interacting with it. Trajectories were computed using an instantaneous snapshot of the vector field, and the FTLEs were

Journal of Experimental Biology (2019) 222, jeb192518. doi:10.1242/jeb.192518

computed on a regular 128^3 grid using a forward Dormand–Prince (Runge–Kutta) integrator with a relative tolerance of 0.001 and an absolute tolerance of 0.0001. The maximum advection time was limited to 0.1 s, and the maximum number of steps was set to 1000. Passive Lagrangian particles were also added to the numerical simulations to reveal trajectories. Note that the LCSs were calculated using the entire 3D flow field with 2D slices extracted for presentation.

RESULTS

Kinematics

We observed three components of the pulsing cycle of the polyp tentacles as shown in Fig. 1. For all polyp calculations, N=5 and means are presented ±s.d. These measurements consist of (1) an active contraction from an open, relaxed state to a fully contracted, closed stated with a duration of 0.55±0.09 s, (2) a relaxation of the tentacle muscles so that the polyp reopens owing to the passive elastic properties of the tentacles with a duration of 0.71±0.03 s, and (3) a relaxation phase in which the tentacles are fully open until the next contraction with a duration of 0.64±0.27 s. This results in an average pulsing period of 1.89±0.27 s and an average pulsing frequency of 0.54±0.09 Hz. The average length of the polyp tentacles was determined to be 0.41±0.03 cm. The average Re_f for the five corals is 8.55±2.18, where f is the pulsing frequency, ρ is the density of the fluid, L_T is the length of a tentacle, and μ is the dynamic viscosity of the water.

A summary of the kinematic parameters averaged for five polyps over five pulses is given in Table 2. The individual polynomial fits to describe the x,y coordinates along the length of a tentacle as a function of time were always within a distance less than $0.05L_T$ of the actual tentacle location. If time and spatial position are non-dimensionalized using the pulse period tentacle length, the actual tentacle position for each individual is within $0.2L_T$ of the averaged tentacle position. Note that we selected an isolated polyp for numerical simulations that pulsed at Re_f=20. We used this particular polyp for comparison with numerical simulations, which were also performed at Re_f=20. This selection was made as the experimentally measured flow fields were the best resolved because there was no interference from neighboring polyps.

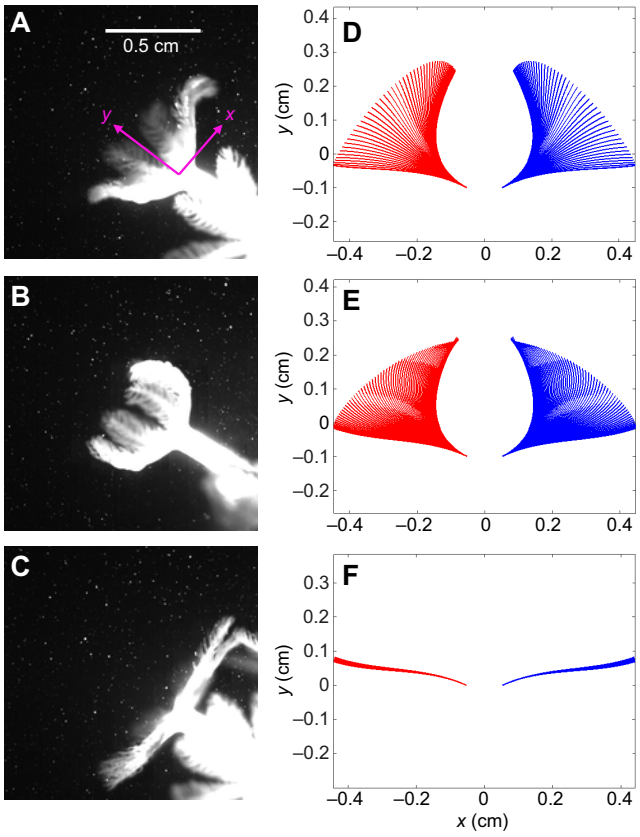

Fig. 1. Tentacle motion of a pulsing xeniid coral polyp. Snapshots taken from a single xeniid coral polyp during tentacle contraction (A), expansion (B) and relaxation before the subsequent contraction (C). Position of a tentacle over time was tracked (in five different polyps for five different pulses), and the motion was fit with time varying polynomials and then averaged to describe the contraction (D), expansion (E) and relaxation (F). Red lines correspond to the leftmost tentacle at different instances in time, and the blue lines correspond to the rightmost tentacle. The base of the polyp is not shown and is assumed to be fixed.

Flow field generated by a single polyp

Fig. 2 and Movie 1 show the velocity vector field generated from a real polyp (Fig. 2A) and within a 2D slice of a three-dimensional numerical simulation (Fig. 2B). Both the real and the simulated polyp operate at Re_f=20. The tentacle motion of the simulated polyp was constructed from the averaged motion of five polyps, as described above. A dominant vertical jet is observed during the entire pulse cycle (Fig. 2, i–vi). Flow is pulled in the horizontal (radial) direction towards the polyp and then up and away from the tentacles. This flow pattern includes minimal back flow, which allows for the sampling of new fluid throughout the pulsing cycle. Note that when the tentacles are closed at the end of contraction and the beginning of expansion (Fig. 2, iii–iv), flow moves downward between the tentacles and upwards into the jet directly above the tentacles. The direction of this jet is aligned with the polyp's stem axis and is very narrowly delimited (about the width of the closed polyp).

Fig. 3 shows a color map of the vorticity and streamlines within a 2D slice cut through the central axis of the polyp for both the real polyp (Fig. 3A) and a numerical simulation (Fig. 3B) at Re_f=20. Unless otherwise noted, the following description of flow features are present for both the experimental measurements and the numerical simulation. Before contraction begins, a stopping vortex ring is visible above the open tentacles (Fig. 3, vi). At the beginning of contraction, an oppositely spinning starting vortex ring is formed at the tips of the tentacles (Fig. 3, i–ii). Towards the end of contraction and beginning of expansion (Fig. 3, iii–iv), the vortex ring moves to the outer surface of the tentacles and is advected up and away from the central axis. The presence of this vortex ring enhances the upward jet because it rotates so that the fluid in the center of the ring is pushed upward (Fig. 3, iv–v). Note that the

Table 2. Summary of experimental data measured from five polyps

Name	Variable	Units	Value
Pulsing period	T	s	1.89±0.27
Duration of contraction	T_c	s	0.27±0.09
Duration of expansion	T_e	s	0.71±0.03
Resting time	T_r	s	0.64±0.27
Tentacle length	L_T	cm	0.41±0.03
Reynolds number	Re_f	–	8.55±2.18
Fluid density*	ρ	kg m^{-3}	1.023×10^3
Fluid dynamic viscosity*	μ	kg ms^{-1}	1.08×10^{-3}

N=5 for polyp specific measurements. Means are presented ±s.d. *Note that ρ and μ were not measured but taken as typical marine values for Re calculations and numerical simulations.

Journal of Experimental Biology (2019) 222, jeb192518. doi:10.1242/jeb.192518

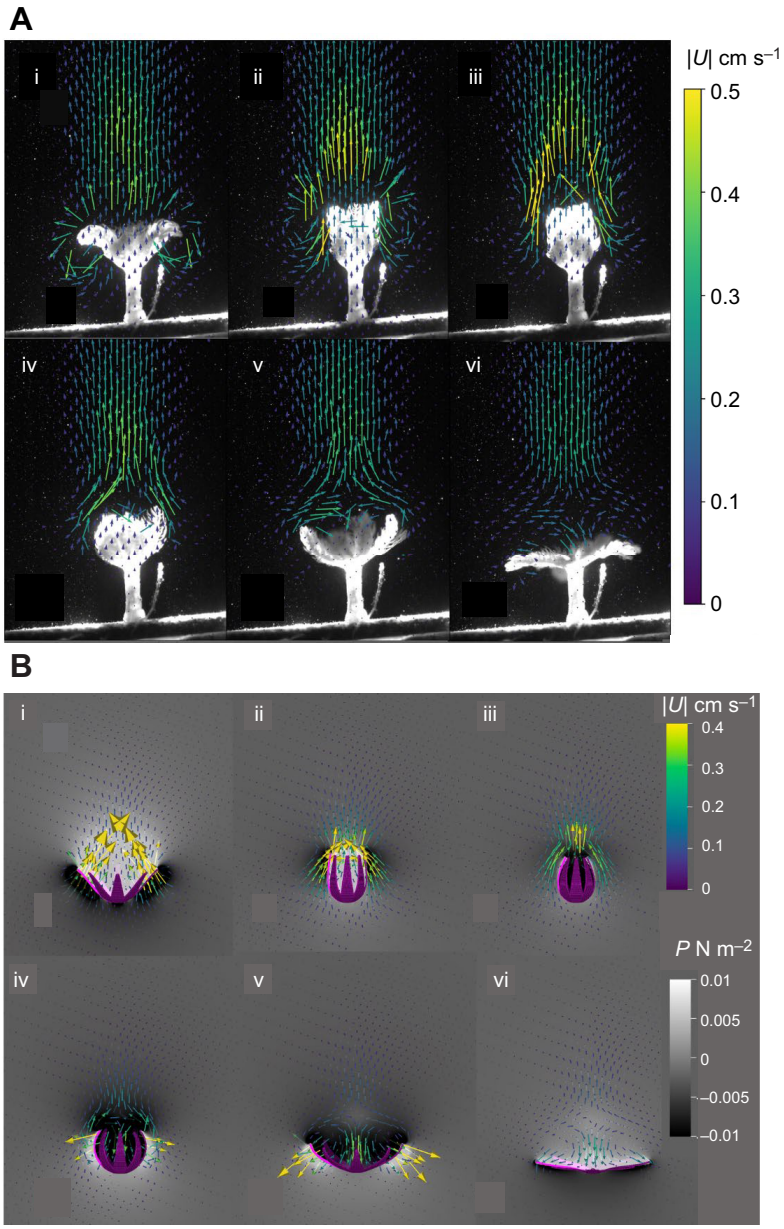

Fig. 2. Flow fields generated by a pulsing xeniid coral polyp. Velocity vector fields from particle image velocimetry (PIV) (A) and from a simulated xeniid coral polyp (B) combined with a pressure (P) color map (B only) during one pulsing cycle. Snapshots are taken at 33% (i), 66% (ii) and 100% (iii) of the contraction and at 33% (iv), 66% (v) and 100% (vi) of the expansion. Vectors show the magnitude ($|U|$) and direction of flow. The arrows correspond to the direction of flow, and the length and colors of the arrows correspond to the magnitude of the velocity. This simulated velocity field was taken from the 10th pulse of the simulation on a 2D slice through the central axis of the polyp. Note that the dynamic viscosity of the fluid was altered to match this particular real polyp ($Re_f \approx 20$).

rotation on the left side of the vortex ring is counterclockwise so that the direction of flow towards the center is upward. Similarly, the rotation on the right side of the vortex ring is clockwise so that the motion towards the center of the polyp is also upward. During expansion, an oppositely spinning stopping vortex is formed at the tips of the tentacles that drives mixing within the polyp (Fig. 3B, iv–vi). It can be observed in the simulation that the flow above the polyp is pulled upward between the starting and stopping vortex rings. At the end of contraction and beginning of expansion in both the experimental and simulation panels (Fig. 3, iii–iv), the stopping vortex is observed. The stopping vortex may only be observed during the remainder of expansion in the numerical simulation as it is not visible in the experiment (it is hidden behind the polyp tentacles).

Fig. 4 provides a comparison of average flow velocities in a real (Fig. 4A–C) and numerically simulated (Fig. 4D–F) polyp over 10 pulsing cycles at Re_f=20. Fig. 4A,D shows the horizontal positions over which the vertical component of the fluid velocity in the upward jet was averaged. The vertical lines show the horizontal positions over which the horizontal (radial) component of the flow moving towards the polyp was averaged. Note that because we use the x, y, z coordinate system, positive horizontal flow is towards the center of the polyp. Fig. 4B,E shows the vertical velocity averaged along the horizontal lines for the live polyp (Fig. 4B) and the numerical simulation (Fig. 4E). Both the PIV and the numerical simulations reveal a strong and nearly continuous upward jet with a maximum spatially averaged vertical velocity of approximately 0.25 cm s^{-1} for the live polyp and 0.2 cm s^{-1} for the simulation. The PIV results show that the vertical velocity never goes below 0.1 cm s^{-1}. Further, the PIV results give the time-averaged vertical volumetric flow rate estimated along the line directly above the contracted tentacle tips to be 0.71 cm^3 s^{-1} with 0% back flow. The vertical velocity decays faster in the numerical simulation than in the live polyp with increasing vertical distance from the coral. Fig. 4C,F shows the horizontal velocity averaged along the three vertical lines as a function of time for the live and simulated polyps, respectively.

Journal of Experimental Biology (2019) 222, jeb192518. doi:10.1242/jeb.192518

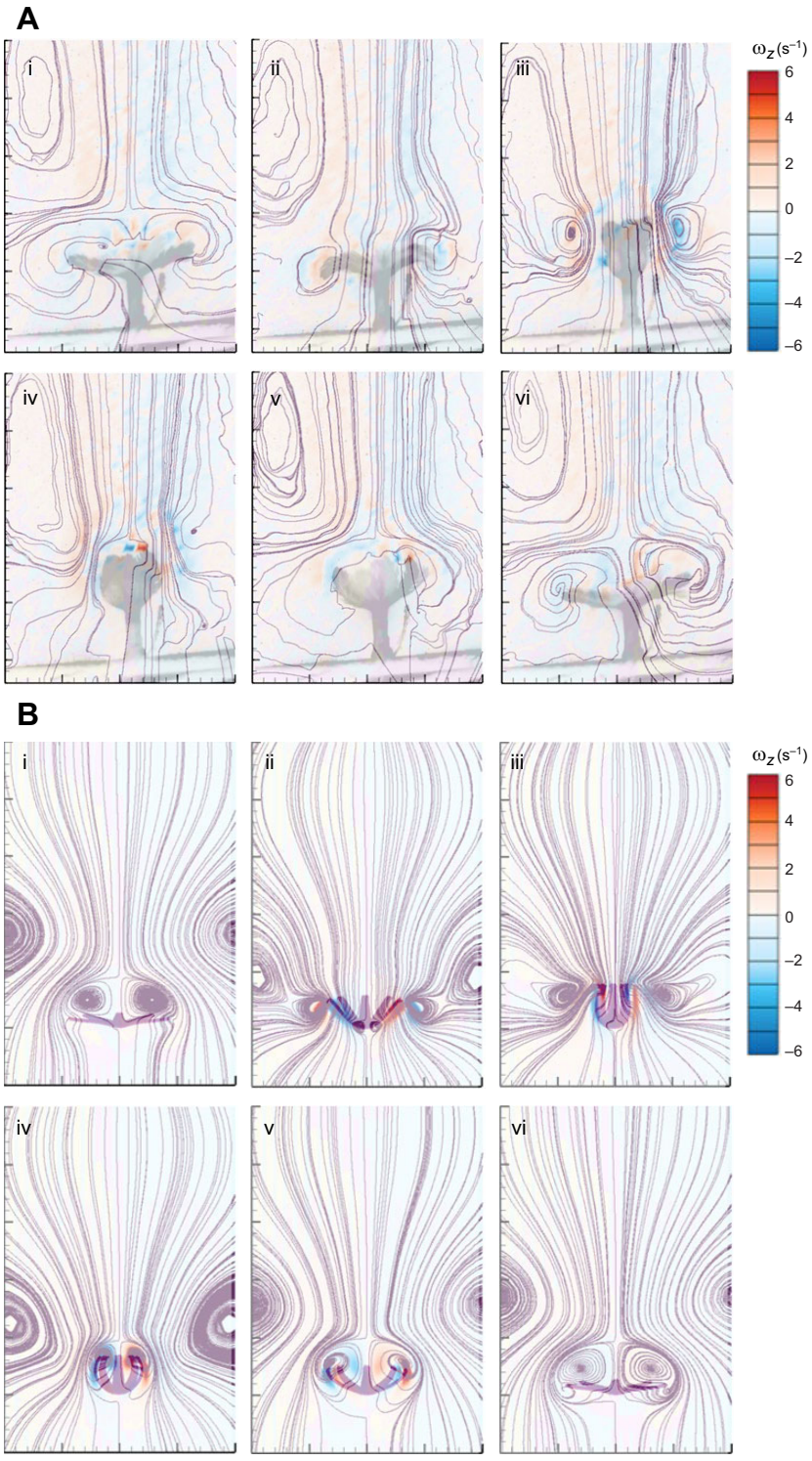

Fig. 3. Flow trajectories generated by a pulsing xeniid coral polyp. Streamlines and vorticity calculated from a 2D velocity field taken in a 2D plane through the central axis of a real xeniid coral polyp (A) and a numerical model (B) during one pulsing cycle. Snapshots are taken at 33% (i), 66% (ii), and 100% (iii) of the contraction and at 33% (iv), 66% (v) and 100% (vi) of the expansion. The color map corresponds to the value of the vorticity (ω_z; red corresponds to counterclockwise and blue to clockwise flow). The simulated velocity field was taken from the 10th pulse of the simulation. Note that the dynamic viscosity of the fluid was altered to match this particular real polyp ($Re_f \approx 20$).

The maximum spatially averaged horizontal (radial) velocity near the tentacle tips (dark blue line) is approximately 0.05 cm s^{-1} for the live polyp and approximately 0.03 cm s^{-1} for the numerical simulation. The time-averaged radial volumetric flux estimated at the tips of the extended tentacles in the PIV results is 0.15 cm^3 s^{-1} with 3.4% back flow.

Fig. 5 shows the three-dimensional results of the flow field and vorticity generated during one pulsing cycle of a simulated coral polyp at Re_f=20. The top row of this figure shows contours of the magnitude of the vorticity and velocity vectors. Vortices form around each tentacle during the contraction. At the end of the contraction, these vortices separate from the tentacles and form a vortex ring that is advected upwards. During the expansion, oppositely spinning vortices form around each tentacle. The velocity vectors show the continuous upward jet in addition to horizontal flow between the tentacles. The middle row shows a color map of the vertical velocity on a 2D slice taken right above the coral (corresponding to the dark blue horizontal line in Fig. 4D). Strong upward flow (red) is observed during the contraction and resting phases. Downward flow (blue) is observed between the tentacles during the expansion. Note that

Journal of Experimental Biology (2019) 222, jeb192518. doi:10.1242/jeb.192518

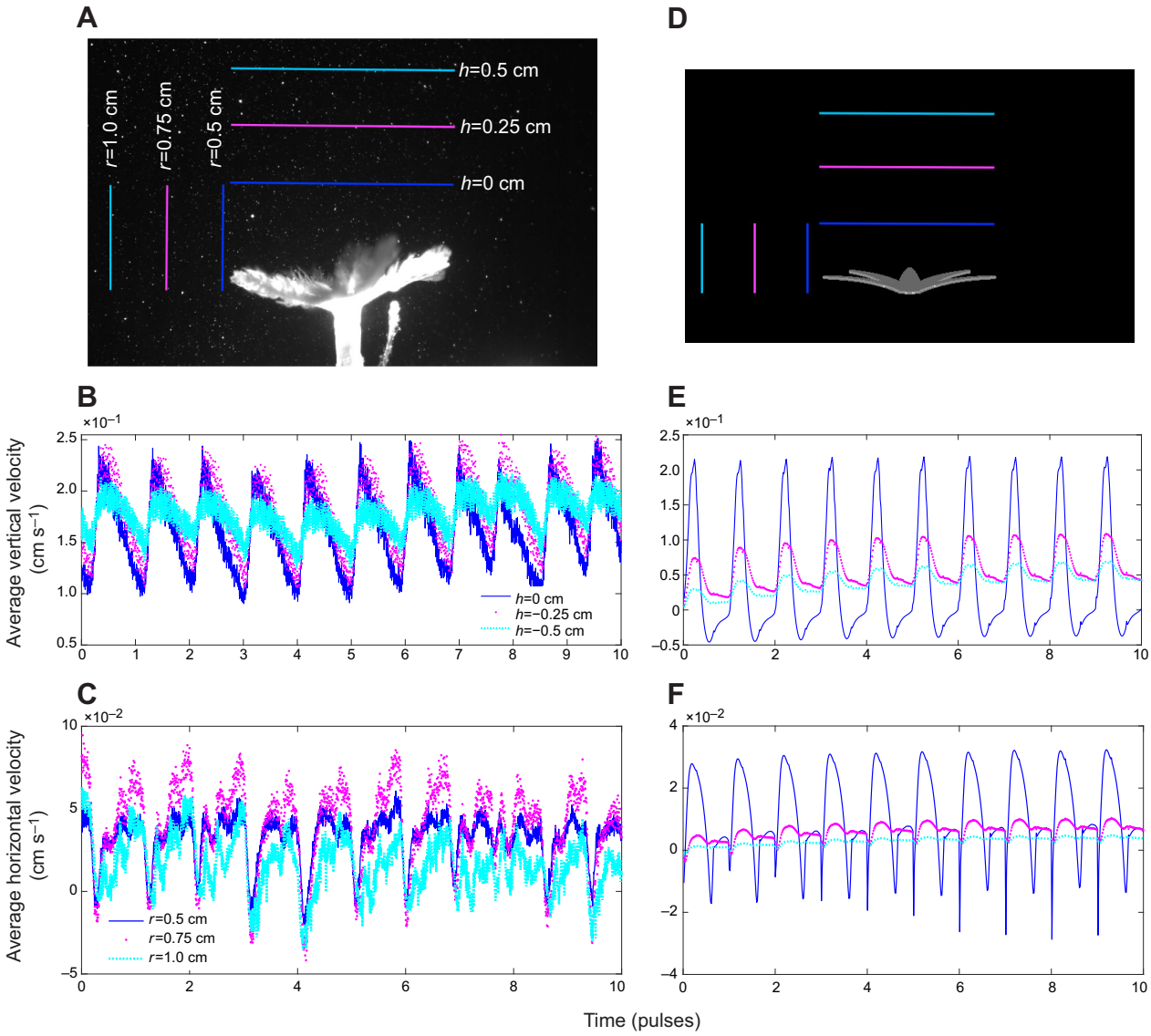

Fig. 4. Vertical and horizontal flows generated by a pulsing xeniid coral. Comparison of flow velocities spatially averaged along a line in the *x*–*y* plane in a real (A–C) and a numerically simulated (D–F) xeniid coral polyp over 10 pulsing cycles. Because the model is based on an average polyp, the dynamic viscosity of the fluid in the simulation was reduced to match the *Re* of this particular polyp ($Re_f \approx 20$). A and D show the horizontal positions over which the vertical flow away from the polyps was averaged at the top of the tentacles at the end of contraction (dark blue) and at positions that are approximately one-half (magenta) and approximately a full (cyan) tentacle length away. The vertical lines show the radial positions over which the horizontal component of the flow was averaged. These positions are at the tip of the tentacle when it is fully relaxed (dark blue) and at positions that are approximately one-half (magenta) and approximately a full (cyan) tentacle length to the left. B and E show the vertical velocity averaged along the horizontal lines at the same three positions for the live polyp (B) and the simulation (E). C and F show the horizontal velocity averaged along the three vertical lines for the live (C) and simulated (F) polyp.

upward flow is seen outside of the tentacles during the expansion, which maintains the upward jet farther above the polyp. The bottom row shows a color map of the horizontal velocity on a 2D surface taken directly to the left of the coral (corresponding to the blue vertical line in Fig. 4D). The strongest flow towards the polyp is seen near the tentacle (red), and this decays to zero with increasing distance from the tentacle (white). Note that the velocity values along the blue line become negative during expansion. This corresponds to flow away from the tentacles, whereas positive velocity values represent flow towards the tentacles.

Flow-field analysis

Fig. 6 shows contours of the log of the FTLE values, which illustrate the instantaneous LCSs. The contours are shown in a 2D slice through the central axis during one pulsing cycle for a simulated polyp at Re_f=20. Recall that regions of the flow that are attractive have small FTLE values, and regions that are repellant have large FTLE values. The repellant regions separate the volumes of the fluid that are sampled by the organism and those that pass by the organism. During contraction, radial flow is pulled towards the polyp but moves into the upward jet (t=0.025T–0.325T). The large FTLE values around the tentacles indicate that this flow does not mix with the fluid between the tentacles. The FTLE values above the polyp are small, indicating that the flow between the tentacles mixes with the upward jet. During expansion (t=0.475T–0.625T), large FTLE values are observed above the polyp, which show that the region of fluid between the tentacles does not mix with the upward jet. This creates a slow mixing region between the tentacles. Note that the 2D contour slice is through a plane that intersects the tentacles rather than the region between the tentacles. Three-

Journal of Experimental Biology (2019) 222, jeb192518. doi:10.1242/jeb.192518

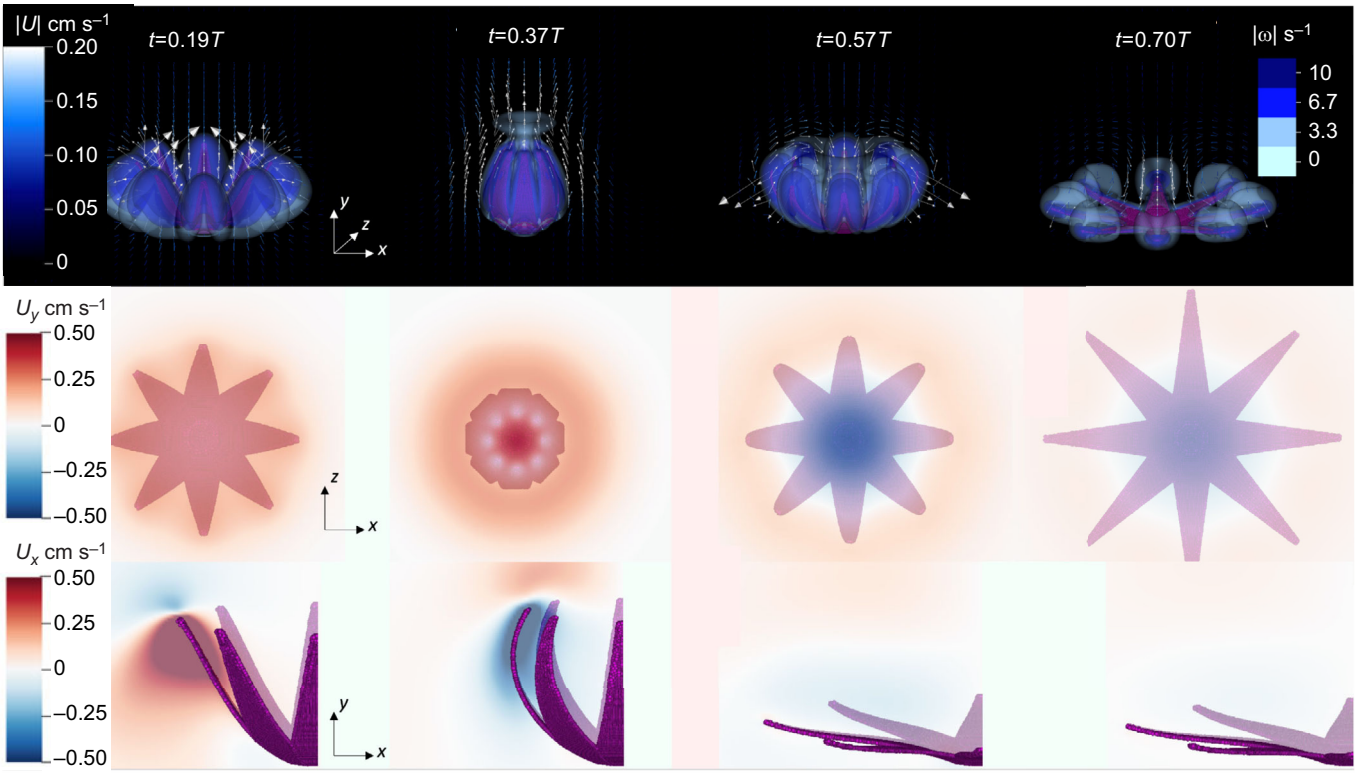

Fig. 5. Three-dimensional flow generated by numerical simulations during the 10th pulsing cycle of a xeniid coral polyp. Top row: fluid velocity vectors and vorticity contours are shown at times that are 19%, 37%, 57% and 70% through the final pulse cycle. Middle row: the vertical velocity on a surface slice right above the coral (the plane falls on the blue horizontal line in Fig. 4D) at the same times as in the top row. Bottom row: the horizontal velocity on a surface directly left of the coral (the plane falls on the blue vertical line in Fig. 4D) at the same times as in the top row.

dimensional visualization of the contours (not shown) reveals smaller FTLEs between the tentacles during expansion. This implies that some new fluid is brought in during the tentacle expansion. Upon the next contraction, this fluid will be expelled upward into the jet and this cycle will repeat itself during the next pulsation. When the polyp is at rest (t=0.775T), the values of the FTLE are small and the fluid is slowly swept over the tentacles and into the upward jet.

To determine how passive tracer particles are pulled towards the corals and moved into the upward jet, untethered immersed boundary points were inserted into the fluid domain in rings centered around the polyp's central axis in the 3D simulated polyp at Re_f=20. These immersed boundary points act as passive, massless tracers that move at the local fluid velocity. These particles were placed in circles with initial radii that were approximately equal to the lengths of the tentacle tips when fully extended and at heights that were equally spaced up to a tentacle length above and below the base of the polyp as shown in Fig. 7 and Movie 2. The movement of the particles is slow and nearly reversible until the particles are close to the polyp or within the narrow vertical jet. This effect is due to the effective low Re away from the polyps (Re<1) as the flow velocities rapidly decay. Once the particles are sufficiently close to the coral, they are either swept over the tentacles or pulled between the tentacles. The particles between the tentacles eventually make it into

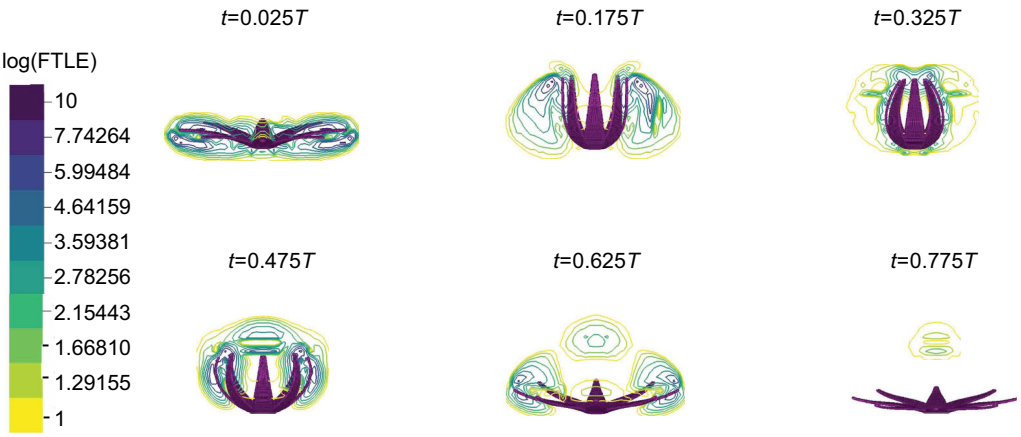

Fig. 6. Contour plot of the finite-time Lyapunov exponents (FTLE) on a logarithmic scale showing the instantaneous Lagrangian coherent structures during one pulsing cycle in a simulated xeniid polyp. Large FTLE regions divide areas of mixing. These are evident around the tentacles because the solid boundary divides the flow field. In addition, the slow flow between the tentacles is separated from the upward jet during expansion (note the blue–purple region above the top of the polyp).

Journal of Experimental Biology (2019) 222, jeb192518. doi:10.1242/jeb.192518

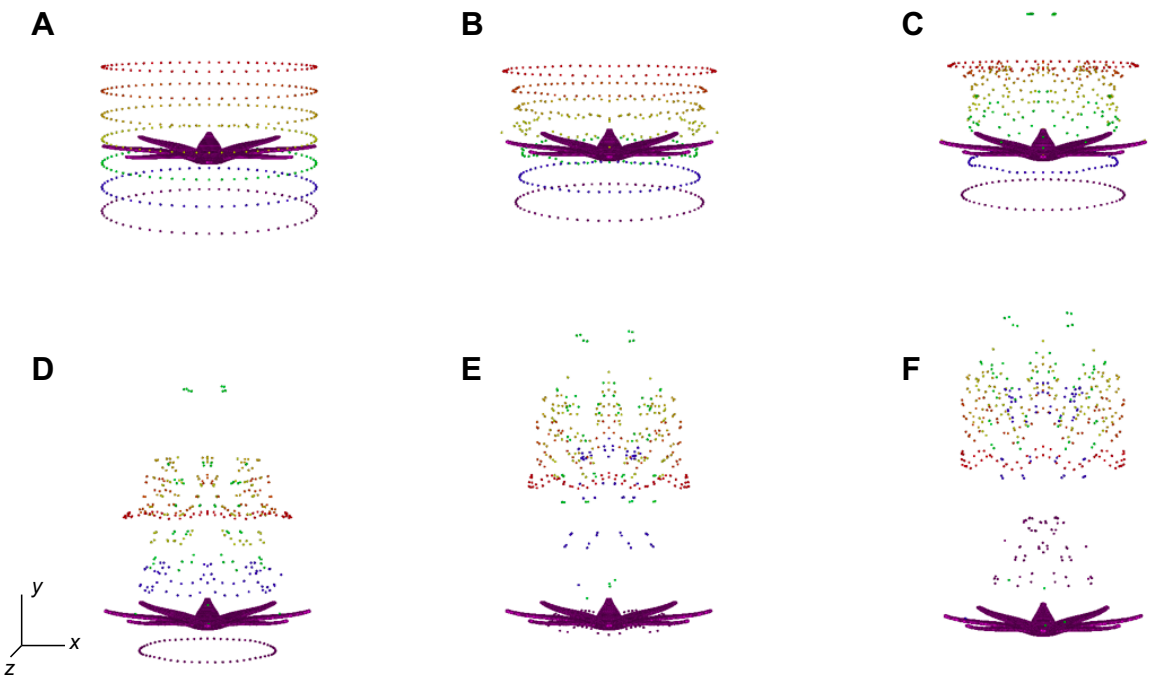

Fig. 7. Temporal snapshots showing the positions of passive Lagrangian tracers initially placed in circles with radii approximately equal to the tentacle length and at vertical positions ranging from a tentacle length below to a tentacle length above the base of the polyp. Times correspond to the particle positions at the beginning of the first (A), third (B), fifth (C), seventh (D), ninth (E) and 11th (F) pulses.

the upward jet after about three to five pulses (or 6–10 s), depending upon their particular trajectories. The residence times for all particles sufficiently close to the coral (those that are pulled between the tentacles and those rapidly swept over the tentacles) range from 3 to 10 s depending upon their particular trajectories.

A comparison of the LCS analysis in Figs 6 and 7 further highlights the dynamics of mass transport. Particles are continually pulled towards the polyp in the radial direction as evidenced by the relatively low values of the FTLEs beyond the boundary layer of the tentacles. The FTLE values are relatively high around each tentacle, and particles in this region are rapidly swept upwards. The FTLE values are lower between tentacles (not shown in the 2D slice passing through the tentacles), and some particles are pulled between the tentacles. Inspection of Movie 2 reveals temporal patterns of particle advection in the vertical direction. During contraction, the values of the FTLEs directly above the oral disk are small, and the particles are pushed upward into the vertical jet. During expansion, the values of the FTLEs are higher, and the particles remain between the tentacles above the oral disk, separated from the upward jet.

Estimation of Péclet number at several scales

To quantify the relative importance of advection and diffusion at various polyp scales, we calculated the *Pe* in different regions of the flow around the corals. Recall that the *Pe* describes the rate of advective transport over the rate of diffusive transport. To consider the relative importance of advection and diffusion of oxygen in water, we set D=2.10×10^{-9} m^2 s^{-1}. To estimate *Pe* for the bulk flow around the whole polyp, we set L to the average tentacle length (0.41 cm) and U to the average vertical velocity in a volume averaged above the coral (3.8×10^{-2} cm s^{-1}) (Samson et al., 2017). This results in *Pe*=740, and the flow at this scale is dominated by advection. To estimate the *Pe* of the flow directly above the central axis and between the tentacles, we set L=0.41 cm and the characteristic velocity equal to the average magnitude of flow within this region such that U=1.4×10^{-2} cm s^{-1} (Samson et al., 2017). This results in *Pe*=270, which corresponds to a flow still dominated by advection.

To estimate *Pe* at the level of the hairs or bristles on the individual tentacles, we measured the bristle diameter and gap between bristles from video in four colonies and on at least three polyps per colony. To calculate this *Pe*, it is necessary to have an estimate of the flow velocity between the bristles. If we know the velocity of the bristles relative to the background flow, the bristle diameter and the gap between bristles, we can estimate the leakiness, l_e, of the bristle array using previous calculations (Cheer and Koehl, 1987). l_e is a measure of the volumetric flow rate between bristles or cylinders relative to the inviscid case. l_e=0 describes a cylindrical array that acts as a solid plate with no flow through it. l_e=1 represents a completely leaky array and corresponds to the inviscid case. In general, lower *Re* and gap-to-diameter ratios correspond to less leaky arrays. The fluid velocity through the array can be estimated as l_eU, where U is the free-stream velocity.

The average diameter of each bristle was 1.74×10^{-2}±3.1×10^{-3} cm, the average distance between bristle centers was 3.34×10^{-2}±4.0×10^{-3} cm, and the average gap-to-diameter ratio was 0.982±0.29. The characteristic length is set to the diameter of the bristle, L=1.74×10^{-2} cm. To approximate the flow between the bristles, we first calculate a bristle-based Reynolds number, Re_b, using a length scale of the bristle diameter and a characteristic velocity given as U_b=0.5$L_T\phi/T$=0.34 cm s^{-1}. ϕ is the angular distance over which the tentacle tip travels each pulse, which is approximated as π radians. This results in Re_b=0.32. The fluid velocity between the bristles can then be calculated as U_b=Ul_e0.034 cm s^{-1}, where l_e=0.1 is the leakiness estimated from Cheer and Koehl (1987). This results in a bristle-based Péclet number Pe_b=23. Note that this Pe_b represents the effective value at the tentacle tips during the pulsing motion. Near the

base of the tentacles and everywhere during the rest period, the velocity of the flow relative to the bristle will be nearly zero such that Pe_b<<1. Thus, the effective Pe_b varies temporally during the cycle and spatially along the tentacle. Accordingly, diffusive transport relative to advective transport may be significant at certain locations and times. To add to the complexity, l_e can also vary with the orientation of the bristles with respect to the flow (Jones et al., 2016), further altering the fluid velocity through the bristles and the effective Pe_b.

Variation in Reynolds number

The numerical results reported thus far correspond to that of the particular isolated polyp at Re_f=20. The average Reynolds number for all polyps measured in this study was lower, Re_f≈10. We highlight the results of 3D simulations at this Reynolds number in Fig. S3. Overall flow patterns and velocities are strikingly similar. Fig. S1A shows a color map of the out-of-plane vorticity, ω_z, and velocity vectors that point in the direction of fluid motion at two snapshots in time during the 10th pulse. Overall, flow patterns are very similar to the Re_f=20 case for the single polyp. Fig. S3B shows a contour plot of the logarithm of the FTLEs at the same two snapshots in time during the 10th pulse, and, similar to the Re_f=20 case, a separated region of mixing between the tentacles is formed during expansion. Fig. S3C,D shows the averaged flow in the vertical and horizontal directions taken along lines that correspond to Fig. 4. The main difference between the higher and lower *Re* cases is that some vertical back flow is observed across the horizontal line taken at the tentacle tips. This is consistent with our earlier study that showed similar flow patterns for pulsing corals where 5<Re_f<40 (Samson et al., 2017).

DISCUSSION

This study provides the first quantitative measurements of the pulsing kinematics and the flows driven by an individual pulsing coral polyp. It also represents the first time that computational fluid dynamics have been used to provide highly resolved flows around these soft corals. Each coral polyp generates a continuous upward jet that lasts during the entire pulsing cycle. The significance of this jet is that oxygen-rich water is advected away from the colony. There is also nearly continual flow towards the coral polyp in the radial direction such that new fluid is brought to the polyp during each pulsing cycle. During the expansion phase, a slow region of mixing, separate from the upward jet, is formed between the tentacles. Each of these flow features occurs at large *Pe*, illustrating the importance of advective transport. Near the boundary layer of the tentacles, the complicated bristled morphology becomes important. We estimate that there is non-neglible flow between the hairs. The relevant Pe_b is on the order of 10^1, such that both diffusive and advective transport are significant at this scale. Finally, LCS analysis and the addition of passive Lagrangian tracer particles show that particles within the boundary layer are continually pulled toward the polyp. Depending on their initial positions, these particles are either rapidly advected over the tentacles and into the upward jet or are brought between the tentacles and eventually pushed upward into the jet.

The combination of flows at different scales ensures that new water is continually brought towards the coral, oxygen-enriched water is continually driven away in an upward jet, and slow mixing between the bristles allows sufficient time for exchange to occur such that oxygen is removed from the tissues. The retention volume between the bristles is needed to allow diffusion of oxygen from the tissue, enriched in oxygen by photosynthesis, to the surrounding water. Without such a retention period or mixing mechanism, the efficiency of advection by the positive vertical jet might be reduced substantially. A similar effect is demonstrated in a separate biological system at similar *Re* and *Pe* in which chemical uptake of an odorant occurs. The marine crab *Callinectes sapidus* flicks its antennules in such a way that new fluid is brought into the hair array during the rapid downstroke and is trapped within the array during the upstroke (Koehl, 2006; Waldrop et al., 2015). This gives sufficient time for odorants to be taken up via diffusion while bringing in new fluid to sample during each flick (Waldrop et al., 2016).

By calculating the average velocity along the tentacle length relative to the ambient fluid velocity during the pulse, we see that the effective Re_b is approximately 0.3 with an average gap-to-diameter ratio of approximately 1. This is within the parameter space in which the bristles rapidly transition from acting like a solid surface to interacting with the fluid like a leaky rake (Cheer and Koehl, 1987). In this transition region, small changes in velocity (Koehl, 2004), changes in the effective bristle spacing owing to flexibility (Waldrop et al., 2015), the instantaneous angle of attack of the array relative to the motion (Jones et al., 2016), and interactions between surfaces (Jones et al., 2016; Loudon et al., 1994) can drastically alter the effective leakiness. We propose that the bristles act more like a solid surface during the expansion, allowing exchange to occur. An effectively more solid structure would be due to the slower velocity of the tentacles relative to flow during expansion (note longer expansion times) and a smaller orientation of the surface relative to flow during expansion (compare the direction of the velocity vectors relative to the tentacles during expansion and contraction in Fig. 2). Both effects would result in lower l_e. We also propose that the tentacles act more like a leaky rake during the faster contraction, bringing in a new volume of fluid. Additional analyses are required to consider how angle of attack, flexibility and tentacle–tentacle interaction might enhance this effect for the parameter space specific to pulsing soft corals.

The only other sessile organism that exhibits a similar active pulsing behavior in the benthos is the upside-down jellyfish, *Cassiopea*, which was reported to generate feeding currents (Santhanakrishnan et al., 2012; Hamlet et al., 2011). The basic flow structures observed here (upward jet and oppositely spinning starting and stopping vortex rings) are similar to those generated by the upside-down jellyfish. These flow patterns are generated in different ways and in different environments. In the case of the soft corals, eight long tentacles expand and contract to pull in fluid between them (see Fig. 5) at relatively low *Re*. For upside-down jellyfish, a shallow bell contracts and expands, similarly generating starting and stopping vortex rings at much higher *Re*, typically on the order of 100 or more. The upward jet is continually pushed through an elaborate array of oral arms. Pulsing soft corals are often found on relatively unsheltered reefs, whereas upside-down jellyfish typically inhabit relatively stagnant estuaries, bays and mangrove swamps. Although both live well within the benthic boundary layer, mass flux between the boundary layers and the free-stream flow will be different.

Pulsing soft corals exhibit an alternative strategy for mixing the diffusive and momentum boundary layers at the centimeter scale to enhance mass transfer. It has been previously shown that corals can actively mix the diffusive boundary layer at the millimeter scale. For example, Shapiro et al. (2014) showed that within the diffusive boundary layer (<2 mm), scleractinian corals can actively enhance mass transport by producing vortical flows driven by epidermal cilia. They propose that this behavior is a survival mechanism during periods of weak ambient flow. Passive mechanisms of mass transfer have also been shown to operate across multiple scales and depend upon colony structure (Shashar et al., 1996). For example, Chang et al.

(2009) measured flow velocities within scale models of branching corals and found morphologies that permitted both high and low flows through the colony. Chamberlain and Graus (1975) used flume experiments with idealized models to show that flow patterns through branching corals depend on colony size, external current velocity and morphological parameters. Unraveling when and under what conditions the active and passive mechanisms of enhanced mass transfer are advantageous could potentially aid in conservation efforts and enhance our understanding of these ecosystems.

Analogous passive and active mechanisms may also be found in other marine and terrestrial organisms to enhance mass transfer. In other cnidarians that harbor symbionts, it is possible that the active motion for swimming could simultaneously enhance photosynthetic rates. For example, the flow patterns observed for pulsing corals (starting and stopping vortices along with a sustained unidirectional jet) are similar to those generated by oblate jellyfish that filter feed and may harbor photosynthetic symbionts (Costello et al., 2008). Alternating starting and stopping vortices are generated during the jellyfish bell contraction and expansion, respectively (Dabiri et al., 2005; Hoover et al., 2017), creating regions of mixing within the bell and strong unidirectional flow over the bell surface. Other examples of active and passive movements to enhance exchange may be found in situations where a nutrient or waste product is in overabundance or underabundance, e.g. the movement of leaves in the wind, which has the effect of reducing the boundary layer and could potentially enhance CO_2 uptake (Schymanski and Or, 2016). Such examples include leaf oscillations in the wind to enhance heat dissipation (Gates, 1965; Grace and Wilson, 1975) and bees flapping their wings to ventilate their hives (Peters et al., 2017).

Acknowledgements
The authors would like to thank the students and staff at the Inter-University Institute, Pierre-Yves Passaggia for his help with LCS, and Boyce Griffith for his assistance with IBAMR.

Competing interests
The authors declare no competing or financial interests.

Author contributions
Conceptualization: J.E.S., L.A.M., R.H., U.S., S.K.; Methodology: J.E.S., L.A.M., D.R., R.H., U.S., S.K.; Software: J.E.S., L.A.M., D.R., U.S., S.K.; Validation: J.E.S., D.R., S.K.; Formal analysis: J.E.S.; Resources: L.A.M., R.H., S.K.; Writing - original draft: J.E.S., L.A.M., S.K.; Writing - review & editing: J.E.S., L.A.M., R.H., U.S., S.K.; Visualization: J.E.S., L.A.M.; Supervision: L.A.M., R.H., U.S., S.K.; Project administration: L.A.M., S.K.; Funding acquisition: L.A.M., S.K.

Funding
This work was supported by National Science Foundation (NSF) PHY grants 1505061 (to S.K.) and 1504777 (to L.A.M.), NSF DMS grant 1151478 (to L.A.M.) and NSF DMS grant 1127914 (to the Statistical and Applied Mathematical Sciences Institute). Travel support for J.E.S. was obtained from a Travelling Fellowship from the Company of Biologists. During this project, J.E.S. was supported by a SAMSI Fellowship and a Howard Hughes Medical Institute International Student Research Fellowship, and by the Women Diver's Hall of Fame for dive training.

Data availability
Data sets in the form of videos are available from the Dryad Digital Repository (Samson et al., 2019): dryad.8mq3896. The immersed boundary software library (IBAMR) is available at https://github.com/IBAMR/IBAMR. The PIV software, OpenPIV, is described in Taylor et al. (2010) and is available at https://github.com/alexlib/openpiv-python. The kinematics acquisition software is described in Hedrick (2008).

Supplementary information
Supplementary information available online at
http://jeb.biologists.org/lookup/doi/10.1242/jeb.192518.supplemental

References
Alben, S. and Shelley, M. (2005). Coherent locomotion as an attracting state for a free flapping body. *Proc. Natl. Acad. Sci. USA* **102**, 11163-11166. doi:10.1073/pnas.0505064102

Bartol, I. K., Krueger, P. S., Thompson, J. T. and Stewart, W. J. (2008). Swimming dynamics and propulsive efficiency of squids throughout ontogeny. *Integr. Comp. Biol.* **48**, 720-733. doi:10.1093/icb/icn043

Battista, N. A., Baird, A. J. and Miller, L. A. (2015). A mathematical model and MATLAB code for muscle–fluid–structure simulations. *Integr. Comp. Biol.* **55**, 901-911. doi:10.1093/icb/icv102

Berger, M. J. and Colella, P. (1989). Local adaptive mesh refinement for shock hydrodynamics. *J. Comput. Phys.* **82**, 64-84. doi:10.1016/0021-9991(89)90035-1

Berger, M. J. and Oliger, J. (1984). Adaptive mesh refinement for hyperbolic partial-differential equations. *J. Comput. Phys.* **53**, 484-512. doi:10.1016/0021-9991(84)90073-1

Bilger, R. W. and Atkinson, M. J. (1992). Anomalous mass transfer of phosphate on coral reef flats. *Limnol. Oceanogr.* **37**, 261-272. doi:10.4319/lo.1992.37.2.0261

Chamberlain, J. A. and Graus, R. R. (1975). Water flow and hydromechanical adaptations of branched reef corals. *B. Mar. Sci.* **25**, 112-125.

Chang, S., Elkins, C., Alley, M., Eaton, J. and Monismith, S. (2009). Flow inside a coral colony measured using magnetic resonance velocimetry. *Limnol. Oceanogr.* **54**, 1819-1827. doi:10.4319/lo.2009.54.5.1819

Cheer, A. Y. L. and Koehl, M. A. R. (1987). Paddles and rakes: fluid flow through bristled appendages of small organisms. *J. Theor. Biol.* **129**, 17-39. doi:10.1016/S0022-5193(87)80201-1

Childress, S. and Dudley, R. (2004). Transition from ciliary to flapping mode in a swimming mollusc: flapping as a bifurcation in re omega. *J. Fluid Mech.* **498**, 257-288. doi:10.1017/S002211200300689X

Childs, H., Brugger, E., Whitlock, B., Meredith, J., Ahern, S., Rugmire, D., Biagas, K., Miller, M., Harrison, C., Weber, G. et al. (2012). VisIt: an end-user tool for visualizing and analyzing very large data. In *High Performance Visualization–Enabling Extreme-Scale Scientific Insight*, pp. 357-372. Berkeley, CA: Lawrence Berkeley National Laboratory.

Costello, J. H. and Colin, S. P. (1995). Flow and feeding by swimming scyphomedusae. *Mar. Biol.* **124**, 399-406. doi:10.1007/BF00363913

Costello, J. H., Colin, S. P. and Dabiri, J. O. (2008). Medusan morphospace: phylogenetic constraints, biomechanical solutions, and ecological consequences. *Invertebr. Biol.* **127**, 265-290. doi:10.1111/j.1744-7410.2008.00126.x

Dabiri, J. O., Colin, S. P., Costello, J. H. and Gharib, M. (2005). Flow patterns generated by oblate medusan jellyfish: field measurements and laboratory analyses. *J. Exp. Biol.* **208**, 1257-1265. doi:10.1242/jeb.01519

Dabiri, J. O., Colin, S. P. and Costello, J. H. (2006). Fast-swimming hydromedusae exploit velar kinematics to form an optimal vortex wake. *J. Exp. Biol.* **209**. doi:10.1242/jeb.02242

Fabricius, K. E. and Alderslade, P. (2001). *Soft Corals and Sea Fans: A Comprehensive Guide to the Tropical Shallow Water Genera of the Central-West Pacific, the Indian Ocean and the Red Sea*. Townsville, QLD: Australian Institute of Marine Science.

Falter, J. L., Lowe, R. J. and Zhang, Z. (2016). Toward a universal mass-momentum transfer relationship for predicting nutrient uptake and metabolite exchange in benthic reef communities. *Geophys. Res. Lett.* **43**, 9764-9772. doi:10.1002/2016GL070329

Gao, H., Feng, L., Qi, N., Berry, C., Griffith, B. E. and Luo, X. (2017). A coupled mitral valve-left ventricle model with fluid–structure interaction. *Med. Eng. Phys.* **47**, 128-136. doi:10.1016/j.medengphy.2017.06.042

Gates, D. M. (1965). Heat transfer in plants. *Scientific Am.* **213**, 76-84. doi:10.1038/scientificamerican1265-76

Gohar, H. A. F. (1940a). Studies on the Xeniiae of the Red Sea: their ecology, physiology, taxonomy and phylogeny. *Publ. Mar. Biol Stn Al-Ghardaqa (Red Sea)* **2**, 24-118.

Gohar, H. A. F. (1940b). The development of some Xeniidae (Alcyonaria) (with some ecological aspects). *Publ. Mar. Biol. Stn Al-Ghardaqa (Red Sea)* **3**, 27-70.

Gohar, H. A. F. and Roushdy, H. M. (1959). On the physiology of the neuromuscular system of *Heteroxenia* (Alcyonaria). *Publ. Mar. Biol. Stn Al-Ghardaqa (Red Sea)* **10**, 91-143.

Gosline, J. M. and DeMont, M. E. (1985). Jet-propelled swimming in squids. *Sci. Am.* **252**. doi:10.1038/scientificamerican0185-96

Griffith, B. E., Hornung, R. D. McQueen, D. M. and Peskin, C. S. (2009). Parallel and adaptive simulation of cardiac fluid dynamics. In *Advanced Computational Infrastructures for Parallel and Distributed Adaptive Applications* (ed. M. Parashar and X. Li), pp. 105-130. Hoboken, NJ: John Wiley and Sons.

Grace, J. and Wilson, J. (1975). The boundary layer over a cottonwood leaf. *J. Exp. Bot.* **27**, 231-241. doi:10.1093/jxb/27.2.231

Haller, G. (2002). Lagrangian coherent structures from approximate velocity data. *Phys. Fluids.* **14**, 1851-1861. doi:10.1063/1.1477449

Hamlet, C., Santhanakrishnan, A. and Miller, L. A. (2011). A numerical study of the effects of bell pulsation dynamics and oral arms on the exchange currents generated by the upside-down jellyfish *Cassiopea xamachana*. *J. Exp. Biol.* **214**, 1911-1921. doi:10.1242/jeb.052506

Hedrick, T. L. (2008). Software techniques for two- and three-dimensional kinematic measurements of biological and biomimetic systems. *Bioinspir. Biomim.* **3**, 034001. doi:10.1088/1748-3182/3/3/034001
Herschlag, G. and Miller, L. A. (2011). Reynolds number limits for jet propulsion: a numerical study of simplified jellyfish. *J. Theor. Biol.* **285**, 84-95. doi:10.1016/j.jtbi.2011.05.035
Hoover, A. P., Griffith, B. E. and Miller, L. A. (2017). Quantifying performance in the medusan mechanospace with an actively swimming three-dimensional jellyfish model. *J. Fluid Mech.* **813**, 1112-1155. doi:10.1017/jfm.2017.3
Jones, S. K., Yun, Y., Hedrick, T. L., Griffith, B. E. and Miller, L. A. (2016). Bristles reduce the force required to 'fling' wings apart in the smallest insects. *J. Exp. Biol.* **219**, 3759-3772. doi:10.1242/jeb.143362
Katija, K., Colin, S. P., Costello, J. H. and Jiang, H. (2015). Ontogenetic propulsive transitions by jetting medusae *Sarsia tubulosa*. *J. Exp. Biol.* **218**, 2333-2343. doi:10.1242/jeb.115832
Koehl, M. A. R. (2004). Biomechanics of microscopic appendages: functional shifts caused by changes in speed. *J. Biomech.* **37**, 789-795. doi:10.1016/j.jbiomech.2003.06.001
Koehl, M. A. R. (2006). The fluid mechanics of arthropod sniffing in turbulent odor plumes. *Chemical Senses.* **31**, 93-105. doi:10.1093/chemse/bjj009
Kremien, M., Shavit, U., Mass, T. and Genin, A. (2013). Benefit of pulsation in soft corals. *Proc. Natl. Acad. Sci. U.S.A* **110**, 8978-8983. doi:10.1073/pnas.1301826110
Lewis, J. B. (1982). Feeding behavior and feeding ecology of the Octocorallia (Coelenterata: Anthozoa). *J. Zool.* **196**, 371-384. doi:10.1111/j.1469-7998.1982.tb03509.x
Loudon, C., Best, B. A. and Koehl, M. A. R. (1994). When does motion relative to neighboring surfaces alter the flow through an array of hairs? *J. Exp. Biol.* **193**, 233-254.
Manuel, J. L. and Dadswell, M. J. (1993). Swimming of juvenile sea scallops, *Placopecten magellanicus* (Gmelin): a minimum size for effective swimming? *J. Exp. Mar. Biol. Ecol.* **174**. doi:10.1016/0022-0981(93)90015-G
Miller, L. A. and Peskin, C. S. (2009). Flexible clap and fling in tiny insect flight. *J. Exp. Biol.* **212**, 3076-3090. doi:10.1242/jeb.028662
Murphy, D. W., Adhikari, D., Webster, D. R. and Yen, J. (2016). Underwater flight by the planktonic sea butterfly. *J. Exp. Biol.* **219**, 535-543. doi:10.1242/jeb.129205
Ngo, V. and McHenry, M. J. (2014). The hydrodynamics of swimming at intermediate Reynolds numbers in the water boatman (Corixidae). *J. Exp. Biol.* **217**, 2740-2751. doi:10.1242/jeb.103895
Nielsen, L. T., Asadzadeh, S. S., Dölger, J., Walther, J. H., Kiørboe, T. and Andersen, A. (2017). Hydrodynamics of microbial filter feeding. *Proc. Natl. Acad. Sci. USA* **35**, 9373-9378. doi:10.1073/pnas.1708873114
Nowell, A. R. M. and Jumars, P. A. (1984). Flow environments of the aquatic benthos. *AnnRev Ecol. Syst.* **15**, 303-328. doi:10.1146/annurev.es.15.110184.001511
Peng, J. and Dabiri, J. O. (2009). Transport of inertial particles by Lagrangian coherent structures: application to predator-prey interaction in jellyfish feeding. *J. Fluid Mech.* **623**, 75-84. doi:10.1017/S0022112008005089
Peskin, C. S. (1972). Flow patterns around heart valves: a numerical method. *J. Comput. Phys.* **10**, 252-271. doi:10.1016/0021-9991(72)90065-4
Peskin, C. S. (2002). The immersed boundary method. *Acta Numer.* **11**, 479-517. doi:10.1017/S0962492902000077
Peskin, C. S. and McQueen, D. M. (1996). Fluid dynamics of the heart and its valves. In *Case Studies in Mathematical Modeling: Ecology, Physiology, and Cell Biology* (ed. H. G. Othmer, F. R. Adler, M. A. Lewis and J. C. Dallon), pp. 309-337. Englewood Cliffs, NJ: Prentice-Hall.
Peters, J. M., Gravish, N. and Combes, S. A. (2017). Wings as impellers: honey bees co-opt flight system to induce nest ventilation and disperse pheromones. *J. Exp. Biol.* **220**, 2203-2209. doi:10.1242/jeb.149476
Petersen, J. K. (2007). Ascidian suspension feeding. *J. Exp. Mar. Biol. Ecol.* **342**, 127-137. doi:10.1016/j.jembe.2006.10.023
Reidenbach, M. A., Monismith, S. G., Koseff, J. R., Yahel, G. and Genin, A. (2006). Boundary layer turbulence and flow structure over a fringing coral reef. *Limnol. Oceanogr.* **51**, 1956-1968. doi:10.4319/lo.2006.51.5.1956
Samson, J. E., Battista, N. A., Khatri, S. and Miller, L. A. (2017). Pulsing corals: a story of scale and mixing. *BIOMATH* **6**, 1712169. doi:10.11145/j.biomath.2017.12.169
Samson, J. E., Miller, L. A., Ray, D., Holzman, R., Shavit, U and Khatri, S. (2019). A novel mechanism of mixing by pulsing corals. *Dryad Digital Repository*. https://doi.org/10.5061/dryad.8mq3896
Santhanakrishnan, A., Dollinger, M., Hamlet, C. L., Colin, S. P. and Miller, L. A. (2012). Flow structure and transport characteristics of feeding and exchange currents generated by upside-down *Cassiopea* jellyfish. *J. Exp. Biol.* **215**, 2369-2381. doi:10.1242/jeb.053744
Schlichter, D. (1982). Epidermal nutrition of the alcyonarian *Heteroxenia fuscescens* (Ehrb.): absorption of dissolved organic material and lost endogenous photosynthates. *Oecologia* **53**, 40-49. doi:10.1007/BF00377134
Schymanski, S. J. and Or, D. (2016). Wind increases leaf water use efficiency. *Plant Cell Environ.* **39**, 1448-1459. doi:10.1111/pce.12700
Shadden, S. C., Lekien, F. and Marsden, J. E. (2005). Definition and properties of Lagrangian coherent structures from finite-time Lyapunov exponents in two-dimensional aperiodic flows. *Physica D.* **212**, 271. doi:10.1016/j.physd.2005.10.007
Shadden, S. C., Dabiri, J. O. and Marsden, J. E. (2006). Lagrangian analysis of fluid transport in empirical vortex ring flows. *Physics Fluids.* **18**, 047105. doi:10.1063/1.2189885
Shapiro, O. H., Fernandez, V. I., Garren, M., Guasto, J. S., Debaillon-Vesque, F. P., Kramarsky-Winter, E., Vardi, A. and Stocker, R. (2014). Vortical ciliary flows actively enhance mass transport in reef corals. *Proc. Natl. Acad. Sci. USA* **111**, 13391-13396. doi:10.1073/pnas.1323094111
Shashar, N., Kinane, S., Jokiel, P. L. and Patterson, M. R. (1996). Hydromechanical boundary layers over a coral reef. *J. Exp. Mar. Biol. Ecol.* **199**, 17-28. doi:10.1016/0022-0981(95)00156-5
Skorczewski T, Griffith B. E., Fogelson A. L. (2014). Multi-bond models for platelet adhesion and cohesion. In *Biological Fluid Dynamics: Modeling, Computation, and Applications. Contemporary Mathematics* (ed. S. D. Olson and A. T. Layton), pp. 149-172. Providence, RI: American Mathematical Society.
Taylor, Z. J., Gurka, R., Kopp, G. A. and Liberzon, A. (2010). Long-duration time-resolved PIV to study unsteady aerodynamics. *IEEE Trans. Instrum. Meas.* **59**, 3262-3269. doi:10.1109/TIM.2010.2047149
Tytell, E. D., Hsu, C. Y. and Fauci, L. J. (2014). The role of mechanical resonance in the neural control of swimming in fishes. *Zoology* **117**, 48-56. doi:10.1016/j.zool.2013.10.011
Vogel, S. (1994). *Life in Moving Fluids*, 2nd edn. Princeton, NJ: Princeton University Press.
Vogel, S. (1998). Exposing life's limits with dimensionless numbers. *Physics Today* **51**, 22. doi:10.1063/1.882079
Vogel, S. (2013). *Comparative Biomechanics: Life's Physical World*, 2nd edn. Princeton, NJ: Princeton University Press.
Waldrop, L., Reidenbach, M. and Koehl, M. A. R. (2015). Flexibility of crab chemosensory sensilla enables flicking antennules to sniffing. *Biol. Bull.* **229**, 185-198. doi:10.1086/BBLv229n2p185
Waldrop, L., Miller, L. A. and Khatri, S. (2016). A tale of two antennules: a tale of two antennules: the performance of crab odor-capture organs in air and water. *R. Soc. Interface.* **13**, 20160615. doi:10.1098/rsif.2016.0615